DOI: 10.2507/34th.daaam.proceedings.xxx

INVESTIGATION OF IRREGULAR THERMAL BEHAVIOUR OF ALSI10MG COMPONENTS MANUFACTURED BY LPBF

Alexandra Morvayova, Maria Emanuela Palmieri, Giuseppe Casalino & Luigi Tricarico

This Publication has to be referred as: Morvayova, A[lexandra]; Palmieri, M[aria] E[manuela]; Casalino, G[iuseppe] & Tricarico L[uigi] (2023). Investigation of irregular thermal behaviour of AlSi10Mg components manufactured by LPBF, Proceedings of the 34th DAAAM International Symposium, pp.xxxx-xxxx, B. Katalinic (Ed.), Published by DAAAM International, ISBN 978-3-902734-xx-x, ISSN 1726-9679, Vienna, Austria
DOI: 10.2507/34th.daaam.proceedings.xxx

Abstract

The unique thermal history associated with the LPBF manufacturing process is closely linked to the distinct behaviour exhibited by parts manufactured via this method, which significantly deviates from that of parts produced via conventional techniques. Specifically, AlSi10Mg specimens manufactured via LPBF exhibit a heterogeneous microstructure, unequivocal high-strength properties, and a distinct response to thermal loading. This latter characteristic can be regarded as a crucial parameter in determining the potential applications of LPBF-manufactured AlSi10Mg specimens, as it indirectly indicates the microstructural alterations induced by thermal loading. In this study, we explore the thermal behaviour of AlSi10Mg cylinders produced via L-PBF through physical simulations. Three different thermal cycles were applied to the cylinders, and the imposed and actual temperatures were evaluated and compared. Subsequently, the obtained signal was filtered to eliminate the effects of the PID controller. The filtered signal was then subjected to a thorough analysis, with a focus on comparing the identified peaks with the distinct thermal behaviour previously reported in the literature for LPBF AlSi10Mg specimens. These identified peaks were subsequently linked to temperature-induced microstructural changes. The noteworthy correlations established in this investigation can be perceived as foundational knowledge for tailoring the heat treatment processes applied to LPBF-manufactured AlSi10Mg parts.

Keywords: thermal behaviour; physical simulation; LPBF; AlSi10Mg.

1. Introduction

Prominent progress in process reliability, productivity and product quality over past years can be perceived as the major reasons for the increasing popularity of LPBF processes in automotive and aerospace industries, especially in the production of parts with high strength-to-weight ratio and intricate designs [1], [2], [3].

The specific, and highly complex nature of this manufacturing technology however facilitates the strongly distinctive characteristics of the manufactured parts, that significantly differ from those ones of the same materials but processed conventionally. Currently, a high number of researchers describe the particular associations within the compounded

process-structure-property interrelationship of the parts manufactured by LPBF, however, this area still needs a more thorough understanding [4], [5].

Notably, it is already generally recognised that a good part of the unique characteristics of LPBF parts can be associated with their solidification conditions with rapid cooling rates, reheating thermal cycles and overall complex thermal history, and their consequent fine-grained and heterogeneous microstructure. To contribute to the better comprehension of the threefold interrelationship underlying the LPBF manufacturing process, and to improve the overall applicability of this manufacturing technology in various industries, rigorous knowledge of the specific behaviour of components manufactured by LPBF is considered crucial [6], [7], [8].

The behaviour of LPBF-manufactured specimens under thermal loads can be perceived as an important parameter for their prospective application and can indirectly indicate the microstructural changes within the specimens caused by thermal loads. The lack of existing research studying the behaviour of LPBF-manufactured specimens under thermal load is reflected in the current practice of thermal treatment of LPBF-manufactured specimens, where rather conventional types of treatment are still applied. It should be noted that fundamental differences between the conventionally manufactured specimens, and specimens manufactured by LPBF make the traditional types of thermal treatment often no longer effective [9], [10].

The present study investigates the thermal behaviour of AlSi10Mg cylinders manufactured by L-PBF using physical simulations. The AlSi10Mg cylinders were subjected to 3 different thermal cycles, where imposed and the real temperature of the cylinders were compared. Subsequently, the received signal was filtered with the simulated influences of the PID controller. The filtered signal was then closely analysed, comparing the identified peaks with the unique thermal behaviour of LPBF AlSi10Mg specimens found in the literature. The identified peaks were further associated with temperature-induced microstructural changes.

2. Materials and methods

Three cylindrical specimens with a diameter of 12 millimetres and a total length of 120 millimetres (Fig. 1) were fabricated by Laser Powder Bed Fusion (L-PBF) using EOSINT M270 machine (EOS, Germany). The specimens were manufactured from gas-atomized virgin AlSi10Mg powder, supplied by EOS. The employed processing parameters are represented in Table 1. The specimens were positioned in a vertical direction, and a zigzag scanning strategy, with a rotation angle of 67° between consecutive layers was employed.

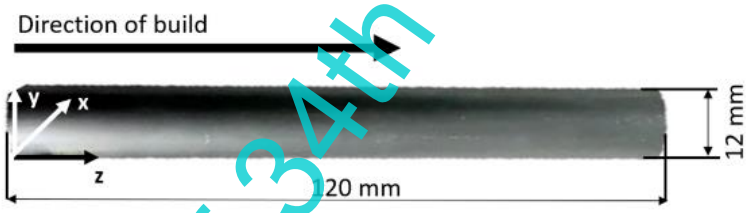

Fig. 1. L-PBF manufactured AlSi10Mg cylinder

Laser power[W]	**Scanning speed** [mm/s]	**Layer thickness** [mm]	**Hatch space** [mm]
275	400	0,03	0,08

Table 1. L-PBF processing parameters

Three different types of thermal loads were applied using the Gleeble 3800 physical simulator, as outlined in Table 2. The thermal loads included a heating phase (from 20 °C to 500 °C), a holding phase (maintaining a constant temperature of 500 °C), and a cooling phase (from 500 °C to 20 °C). It is important to note that subsequent analysis revealed that the physical simulator was unable to achieve the desired cooling rate, thus the thermal behaviour during the cooling phase could not be evaluated. The physical simulation system employed two thermocouples: one for heating the specimen using Joule heating principles, and another to measure the instantaneous temperature of the specimen (Fig. 2).

Thermal load	Heating rate [°C/s]	Keeping phase time [s]	Cooling phase [°C/s]
TH1	10	60	10
TH2	7.5	80	7.5
TH3	6	240	6

Table 2. Imposed thermal loads

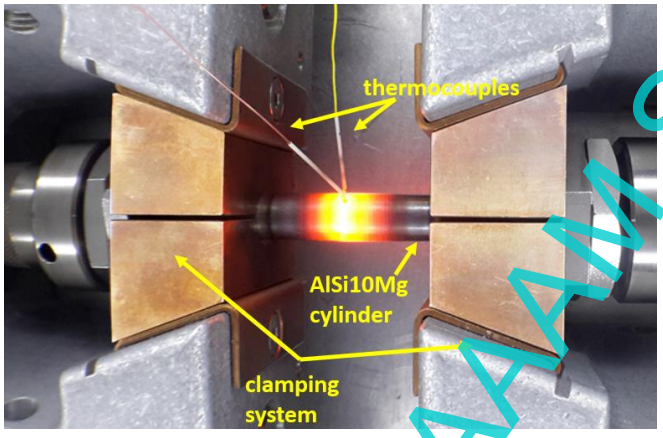

Fig. 2. AlSi10Mg cylinder during physical simulation

The measured (T_m) and imposed (T_i) temperatures were subsequently analysed, their difference (T_{diff}) for each time step was calculated (1), and the T_{diff} over the imposed temperature was plotted.

$$T_{diff} = T_m - T_i \tag{1}$$

3. Filtering of the signal

The signal of received temperature deviation, plotted over the real temperature was thereafter filtered from the influence of the PID controller, used for process control in the applied physical simulator.
The influence of the PID controller for each case of applied thermal loads was simulated in Comsol Multiphysics, according to the standard PID control algorithm (2) [11], [12].

$$u(t) = u_{bias} + k_p[c_{set}(t) - c(t)] + k_i \int_0^t [c_{set}(t) - c(\tau)]d\tau - k_d \frac{d}{dt} c(t) \tag{2}$$

Where u_{bias} stands for bias of PID, k_p is the proportional gain, c_{set} is the reference value and k_d is a derivative gain.
Furthermore, the filtering of the derivative was enabled. The PID control parameters were used according to the real characteristics of the PID controller applied in the physical simulator.

4. Results and discussions

Fig. 3 shows the comparison of raw, unfiltered signal of T_{diff}, plotted over the imposed temperature.

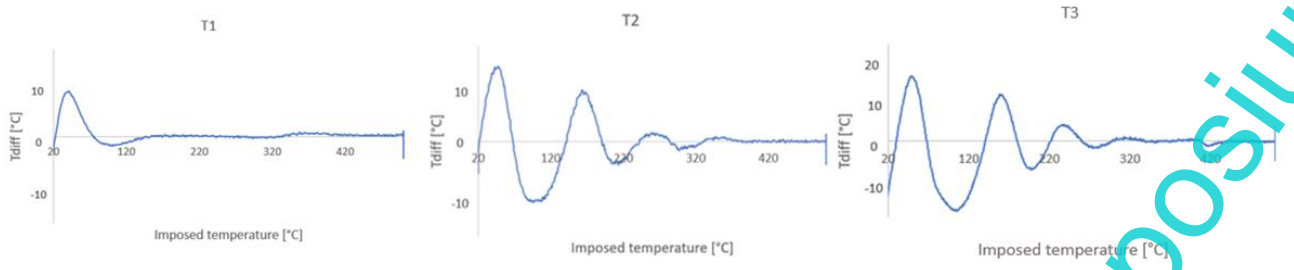

Fig. 3. Comparison of unfiltered T_{diff}, plotted over time in specimens under different types of thermal load

Significant differences between the plotted curves of different thermal loads were observed already in the unfiltered state. The cylinder under thermal load with the highest heating rates demonstrated the least irregularities, and as the heating rate increased, more irregularities were observed. All of the observed curves initially demonstrated similar irregularities, starting with a larger peak in a positive direction, immediately followed by a negative peak. It should be noted that the height of the first peak correlated with the initial deviation at Ti=20 °C. The deeper the initial deviation, the higher the initial peak, suggesting that it was attributed to the PID controlling compensating for the higher initial temperature of the specimen than was the temperature set. The same applies to the second negative peak, where the lower initial deviation resulted in more shallow peaks. It should be also noted that lower heating rates (T2, T3) resulted in more peaks than thermal load with the higher heating rate (T1).

Fig. 4 shows curves of Tdiff plotted over the imposed temperature of cylinders under different thermal loads, already filtered from the influence of the PID controller.

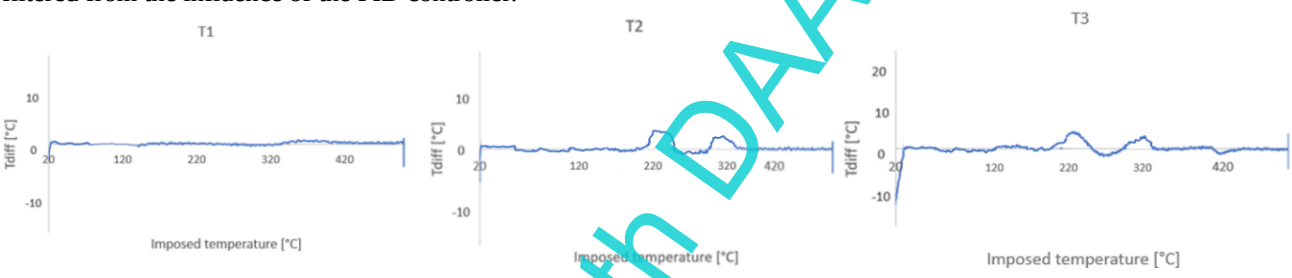

Fig. 4. Filtered signal of T_{diff} plotted over the imposed temperature for different heating rate

It should be noted that the number of irregularities identified in the signal correlated with the applied heating rate. The temperature of the specimen under the thermal load T1 mimicked the imposed temperature most accurately, resulting in the least number of irregularities. The irregularities between the temperature of the AlSi10Mg cylinder and the imposed temperature of the T1 load were located mainly until 120 °C, consisting of numerous very short peaks. Another irregularity in the analysed temperature was observed between 320°C and 400°C. The observed peak has a positive direction and prolonged, short, and doltish shape.

Two main irregularities between the real temperature of the AlSi10Mg cylinders and the temperature imposed in the T2 thermal load were observed. The first positive peak was identified between 210 °C and 280 °C, and the second positive peak was identified between 300 and 350 °C. Both peaks demonstrated similar shape characteristics, however, the first identified peak was slightly higher and thicker. It should be noted that the temperature of the cylinder between both identified peaks (280-300 °C) relatively closely followed the imposed temperature and thus no significant irregularities in this temperature range were identified.

Similar irregularities were identified between the temperature of the AlSi10Mg specimen and the imposed temperature of thermal load T3. The first positive peak was identified at a slightly lower temperature than previously, starting at around 190 °C. It is noteworthy that, unlike in the thermal load T2, the first and second peaks are seemingly connected with a shallow negative peak, occurring between 270 and 290 °C. The second positive peak was subsequently identified between 290 and 340 °C. An additional negative peak was identified between 410 and 440 °C.

The first peak, observed in cylinders under T2 and T3 thermal loads, has been, according to Van Cauwenbergh et al. [14] attributed to microstructural changes induced by thermal loading. These changes are primarily characterized by the precipitation of silicon (Si) particles from the supersaturated aluminium (Al) cells. The missing of the first peak during the analysis of the first thermal load indicates that the applied heating rate did not provide sufficient activation energy for this change to fully occur.

Similarly, the second peak, observed during all three thermal loads, is also linked to temperature-induced microstructural alterations. Within this temperature range, the microstructural changes involve both diffusional activity and spheroidization of the Si particles [13], [14], [15].

The third peak, observable during T3 thermal load can be attributed to the coalescence of the primary Si particles. It should be noted that this microstructural transformation requires a higher activation energy, and consequently, it only manifests at elevated temperatures with sufficiently low heating rates [16].

It should be noted that the exact position and shapes of the identified peaks also depend on the applied heating rate, correlating to the total thermal energy delivered to the specimen under the respective thermal load. Thermal loads with lower heating rates deliver the thermal energy sufficient to activate the respective microstructural change sooner, and thus the peak occurs at a slightly lower temperature [17].

5. Conclusions

The present study investigates the thermal behaviour of 3 AlSi10Mg cylinders under different thermal loads. The study includes filtering of the received signal from the influences of the PID controller using numerical simulation. Analysis of the filtered temperature of each L-PBF manufactured cylinder under the thermal loads has provided several conclusions.

- The PID controllers might substantially influence the difference between imposed and real temperature measured in the cylinder under thermal load. Thus, in order to unambiguously analyse the irregularities between the temperature of the cylinders and the imposed temperature, the influence of the PID controller must be considered.
- The behaviour of AlSi10Mg cylinders manufactured by L-PBF under thermal load is influenced by the applied heating rate, where lower heating rates result in more observable irregularities between the imposed and immediate temperature of the specimen. The applied heating rate also influences the total thermal energy delivered to the cylinder under thermal load and thus influences the exact position and shapes of the identified peaks.
- The first identified peak, observed between 210-280 °C in cylinders under T2 and T3 thermal loads can be attributed to the precipitation of Si particles from supersaturated Al cells.
- The second identified peak, observed between 300-400 °C in cylinders under all can be attributed to diffusional activity and spheroidization of Si particles.
- The third identified peak, occurring between 410-440 °C in a cylinder under T3 thermal load can be attributed to the coalescence of the primary Si particles.

Investigating the thermal behaviour of AlSi10Mg components manufactured using L-PBF under thermal load and establishing a correlation between the observed irregularities and the microstructural changes caused by temperature, has the potential to become a crucial element in identifying the complex process-structure-property relationship in L-PBF processes of the AlSi10Mg alloy. The distinguished correlations can be further applied as a base knowledge for tailoring the heat treatment for LPBF-manufactured AlSi10Mg parts.

6. References

[1] Abd-Elaziem, W., Elkatatny, S., Abd-Elrahim, A., Khedr, M., Abd El-baky, M. A., Hassan, M. A., Abu-Okail, M., Mohammed, M., Järvenpää, A., Allam, T., & Hamada, A. (2022). On the current research progress of metallic materials fabricated by laser powder bed fusion process: a review. Journal of Materials Research and Technology, 20, 681-707.

[2] Kroft, L.; Bicova, K[aterina] & Milsimerova, A[neta] (2020). Use of 3D Printing Technology in Teaching the Basics of Milling Technology, Proceedings of the 31st DAAAM International Symposium, pp.0323-0327, B. Katalinic (Ed.), Published by DAAAM International, ISBN 978-3-902734-29-7, ISSN 1726-9679, Vienna, Austria

[3] Casalino, G., Campanelli, S. L., Contuzzi, N., & Ludovico, A. D. (2015). Experimental investigation and statisticaloptimisation of the selective laser melting process of a maraging steel. Optics & Laser Technology, 65, 151-158.

[4] Eskandari Sabzi, H., & Rivera-Díaz-del-Castillo, P. E. J. (2020). Composition and process parameter dependence of yield strength in laser powder bed fusion alloys. Materials & Design, 195, 109024.

[5] Morvayová, A., Contuzzi, N., & Casalino, G. (2023). Numerical prediction of lack-of-fusion defects in selective laser melted AlSi10Mg alloy. Materials Science and Technology.

[6] Hyer, H., Zhou, L., Park, S., & Lee, J. (2020). Understanding the Laser Powder Bed Fusion of AlSi10Mg Alloy. Metallography, Microstructure, and Analysis, 9, 484-502.

[7] Caiazzo, F., Alfieri, V., & Casalino, G. (2020). On the Relevance of Volumetric Energy Density in the Investigation of Inconel 718 Laser Powder Bed Fusion. Materials (Basel, Switzerland), 13(3), 538.

[8] Roveda, I., Serrano-Munoz, I., Kromm, A., & Madia, M. (2022). Investigation of residual stresses and microstructure effects on the fatigue behaviour of a L-PBF AlSi10Mg alloy. Procedia Structural Integrity, 38, 564-571.

[9] Padovano, E., Badini, C., Pantarelli, A., Gili, F., & D'Aiuto, F. (2020). A comparative study of the effects of thermal treatments on AlSi10Mg produced by laser powder bed fusion. Journal of Alloys and Compounds, 831, 154822.

[10] Ghasemi, A., Fereiduni, E., Balbaa, M., Elbestawi, M., & Habibi, S. (2022). Unraveling the low thermal conductivity of the LPBF fabricated pure Al, AlSi12, and AlSi10Mg alloys through substrate preheating. Additive Manufacturing, 59(Part A), 103148. https://doi.org/10.1016/j.addma.2022.103148
[11] Armstrong, B., & Wade, B. (2000). Nonlinear PID control with partial state space knowledge: Damping with derivative. International Research, 18(8), 715-731.
[12] Cedro, L., & Wieczorkowski, K. (2019). Optimizing PID controller gains to model the performance of a quadcopter. Transportation Research Procedia, 40, 156-169.
[13] Van Cauwenbergh, P., Beckers, A., Lore, T., Hooreweder, B., & Vanmeensel, K. (2018). Heat Treatment Optimization via Thermo-Physical Characterization of AlSi7Mg and AlSi10Mg Manufactured by Laser Powder Bed Fusion (LPBF).
[14] Marola, S., Calignano, F., Manfredi, D., Ambrosio, E. P., & Biamino, S. (2018). A comparison of Selective Laser Melting with bulk rapid solidification of AlSi10Mg alloy. Journal of Alloys and Compounds, 742, 271-279.
[15] Van Cauwenbergh, P., Samaee, V., Thijs, L., Delroisse, G., & Kruth, J. P. (2021). Unraveling the multi-scale structure-property relationship of laser powder bed fusion processed and heat-treated AlSi10Mg. Scientific Reports, 11(1), 6423.
[16] Cabrini, M., Lorenzi, S., Testa, C., Manfredi, D., Lombardi, M., Aversa, A., Andreatta, F., Fedrizzi, L., Dekhtyar, Y., Sorokins, H., & Biamino, S. (2021). Effect of Heat Treatment on Microstructure and Selective Corrosion of LPBF-AlSi10Mg by Means of SKPFM and Exo-Electron Emission. Materials, 14(19), 5602.
[17] Megahed, S., Bühring, J., Duffe, T., Bach, A., Schröder, K.-U., & Schleifenbaum, J. H. (2022). Effect of Heat Treatment on Ductility and Precipitation Size of Additively Manufactured AlSi10Mg. Metals, 12(8), 1311.